Plasma Velocities in the Heliosheath and the Influence of the Interstellar Wind

by

Chris Chronopoulos

Submitted to the Department of Physics
in partial fulfillment of the requirements for the degree of

Bachelor of Science in Physics

at the

MASSACHUSETTS INSTITUTE OF TECHNOLOGY

June 2009

Author .....
Department of Physics
May 22, 2009

Certified by .....
John W. Belcher
Class of '22 Professor of Physics
Thesis Supervisor

Accepted by .....
Professor David E. Pritchard
Senior Thesis Coordinator, Department of Physics

Plasma Velocities in the Heliosheath and the Influence of the Interstellar Wind

by

Chris Chronopoulos

Submitted to the Department of Physics
on May 22, 2009, in partial fulfillment of the
requirements for the degree of
Bachelor of Science in Physics

Abstract

A new coordinate system (Interstellar Heliospheric Coordinates, or IHC) is introduced to enable the detailed study of the influence of the interstellar wind on the heliosheath. Recent, *in situ* measurements of plasma velocities in the heliosheath by Voyager 2 are projected into the IHC system and analyzed. We consider steady state flows as well as time dependent phenomena, and we show that a transient event with no obvious cause or direction takes a particularly simple form in IHC.

Thesis Supervisor: John W. Belcher
Title: Class of '22 Professor of Physics

Acknowledgments

I would like to thank my advisor John Belcher for giving me the opportunity to work on this exciting project, and for his help with the completion of this thesis. I would also like to thank my family for their continued support throughout my years at MIT. I could never have come this far without their inspiration and guidance.

Contents

List of Figures

Chapter 1

Introduction

1.1 The Heliosphere

The solar wind is a supersonic flow of plasma that originates in the sun's corona. It blows out a bubble in the interstellar medium (ISM) known as the *heliosphere*. The solar wind speed in general depends on time and space, but it varies very little as it travels outward. Typical velocities are about 400 km/s, and the density falls off with the inverse-square of the helioradius, reaching about 7 cm^{-3} at 1 AU.

The solar wind and the surrounding ISM constitute different magnetic field topologies, so they do not mix. Instead they remain separated by an interface known as the *heliopause*. The heliopause is the boundary of the heliosphere and the limit of the sun's material extent.

Because the solar wind is supersonic, it must undergo a shock before colliding with the heliopause. This is the *termination shock*, a supercritical and quasi-perpendicular MHD discontinuity [6] where the solar wind transitions from supersonic to subsonic flow. It lies at a helioradius of about 80-100 AU.

The layer of shocked solar wind between the termination shock and the heliopause is known as the *heliosheath*. It is in the heliosheath that the solar plasma first becomes causally connected to the ISM. One of the consequences of this is the viscous transfer of shear momentum from the interstellar wind to the heliosheath. This should cause the heliosheath plasma to flow tangentially down the *heliotail*, which is the heliosphere's exhaust port. A diagram of the important features of the heliosphere is provided in Figure 1-1.

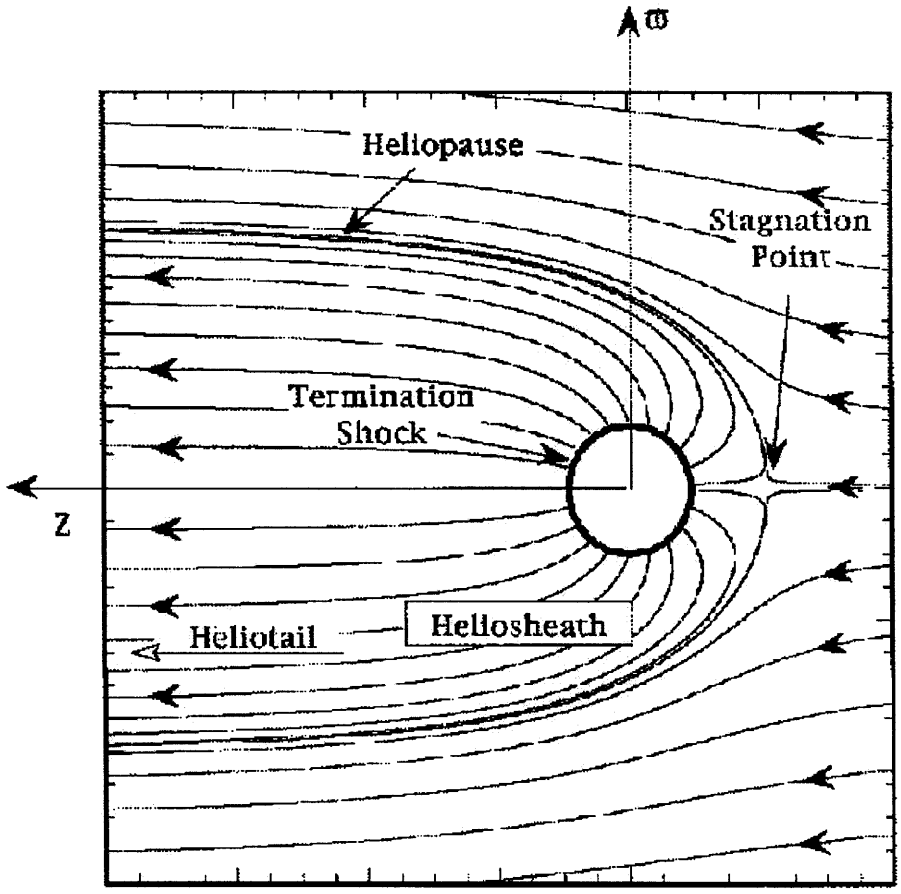

Figure 1-1: The structure of the heliosphere in an interstellar wind [1].

1.2 The Voyager Program

Voyagers 1 and 2 were launched in 1977 to study Jupiter and Saturn. Both probes were able to take advantage of a convenient planetary alignment which allowed them to slingshot into the outer solar system, with Voyager 2 visiting Uranus and Neptune along the way. Each spacecraft was equipped with plasma diagnostic instruments, but the instrument on Voyager 1 malfunctioned shortly after Saturn encounter. Thus when Voyager 1 crossed the termination shock in December 2004, information on heliosheath velocities was limited to two-dimensional estimates provided by the Low Energy Charged Particle detector.

Voyager 2 crossed the termination shock in August 2007 with its plasma instrument fully functional. It has been reporting on plasma parameters in the heliosheath ever since. These are the first three-dimensional pictures of velocity space to become available from the edge of the heliosphere.

1.3 Motivation

Since Voyager 2's crossing of the termination shock, several studies (see for example [6, 7]) have reported on plasma parameters in the heliosheath, including bulk velocity. The predominant coordinate system used in these reports has been the heliographic system (discussed in section 3), which has required the investigators to make assumptions about the approximate location of the interstellar wind stagnation point, and hence the meaning of their results.

The purpose of this thesis is to characterize the velocity field of the heliosheath in a coordinate system that is appropriate to the geometry of the heliosphere under the influence of an interstellar wind. It is our hope that this analysis shines light on some observations that have proved difficult to understand in less physically appropriate coordinate systems, and that it may lend itself naturally to comparison with theoretical models of the heliosheath.

Chapter 2

Data Acquisition and Processing

2.1 The Voyager Plasma Instrument

All of the data presented in this thesis was taken by the Plasma Science Experiment (PLS) aboard Voyager 2 (see Figure 2-1). The instrument consists of four modulated-grid Faraday cups, with the three main cups A, B, and C oriented 20° from the symmetry axis of the cluster, and separated by 120° of azimuth [3].

Figure 2-2 shows a schematic diagram of one of the Faraday cups. Grids 1 and 3 are in contact with the walls of the cup, which is grounded to the spacecraft body. The two separate volumes bounded by grid 1, grid 3, and the walls constitute electrically isolated Faraday cages. For a given energy channel k, the potential of grid 2 is modulated by a square-wave with limits Φ_k and Φ_{k+1} . Modulation is available in two different resolutions, designated L-mode (low resolution) and M-mode (high resolution). The Φ_k's are given by the formulae:

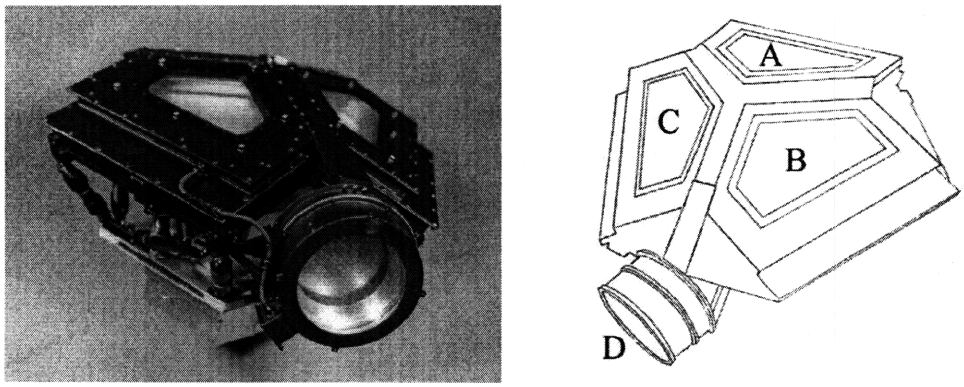

Figure 2-1: Sensor arrangement on the Voyager Plasma Science Instrumnet (PLS) [2].

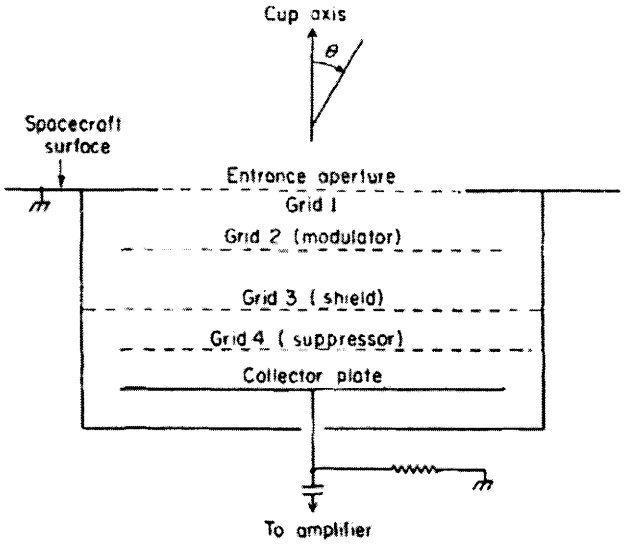

Figure 2-2: Schematic diagram of a modulated-grid Faraday cup [5].

$$\Phi_k = (60(1.33352)^{k-1} - 50) \text{ volts for } k = 1 \text{ to } 17 \text{ in L-mode.} \tag{2.1}$$

$$\Phi_k = (60(1.03663)^{k-1} - 50) \text{ volts for } k = 1 \text{ to } 129 \text{ in M-mode.} \tag{2.2}$$

Finally, grid 4 is maintained at a highly negative potential to reflect the majority of incoming electrons.

The current measured at the collector plate consists of two components. First, there is a steady base value representing the current of protons whose normal velocities v_n satisfy:

$$\frac{mv_n^2}{2q} > \Phi_{k+1} \tag{2.3}$$

where m is the mass of the proton and q is its charge. Second, there is an alternating component which oscillates at the frequency of modulation, but 180° out of phase. The amplitude of the alternating signal represents the channel current I_k of protons whose v_n satisfy [5]:

$$\Phi_k < \frac{mv_n^2}{2q} < \Phi_{k+1} \tag{2.4}$$

The channel currents I_k are then amplified, filtered and integrated before being sampled by an 8-bit logarithmic A/D converter and digitally trasmitted [3].

2.2 The Reduced Distribution Function

Consider the orthonormal basis $\{\hat{n}, \hat{t}_1, \hat{t}_2\}$ of a Faraday cup, where $\hat{n}$ is the cup normal and $\hat{t}_1, \hat{t}_2$ are the transverse dimensions. The measured current I_k is related to the velocity distribution function $f(\overrightarrow{v})$ by

$$I_k = qA \int_{v_k}^{v_{k+1}} v_n dv_n \int_{-\infty}^{\infty} \int_{-\infty}^{\infty} dv_{t_1} dv_{t_2} f(\overrightarrow{v}) G_{\hat{n}}(\overrightarrow{v}) \tag{2.5}$$

where A is the area of the collector plate, $G_{\hat{n}}(\overrightarrow{v})$ is the geometric transmission function of a cup with normal vector $\hat{n}$, and v_k is the velocity of a proton that is just stopped by the potential Φ_k. That is,

$$v_k = \sqrt{\frac{2q\Phi_k}{m}} \tag{2.6}$$

We may simplify Equation 2.5 considerably by making two key approximations. First, the sensor is oriented in such a way that the solar wind is streaming into the cups with a bulk velocity $V_n >> v_{th}$, where v_{th} is the thermal speed. Therefore the fraction of particles approaching the cup with an angle of incidence greater than the cup's field-of-view (which is about 45° [3]) is negligible, and we approximate

$$f(\overrightarrow{v}) G_{\hat{n}}(\overrightarrow{v}) \approx f(\overrightarrow{v}) \tag{2.7}$$

Second, the solar wind is sufficiently warm, and the channel spacing sufficiently small ($v_{th} >> v_{k+1} - v_k$), that $f(\overrightarrow{v})$ is approximately constant over any given channel [2]. Therefore,

$$\begin{aligned} \int_{v_k}^{v_{k+1}} v_n f(v_n, v_{t_1}, v_{t_2}) dv_n &\approx \frac{f(\bar{v}_k, v_{t_1}, v_{t_2})}{2} (v_{k+1}^2 - v_k^2) \\ &\approx f(\bar{v}_k, v_{t_1}, v_{t_2}) \bar{v}_k \Delta v_k \end{aligned} \tag{2.8}$$

where

$$\bar{v}_k = (v_{k+1} + v_k)/2 \qquad \text{and} \qquad \Delta v_k = v_{k+1} - v_k \tag{2.9}$$

Using these approximations, we write

$$I_k \approx qA\bar{v}_k \Delta v_k \int_{-\infty}^{\infty} \int_{-\infty}^{\infty} dv_{t_1} dv_{t_2} f(\bar{v}_k, v_{t_1}, v_{t_2}) \tag{2.10}$$

We recognize the double integral as the reduced distribution function,

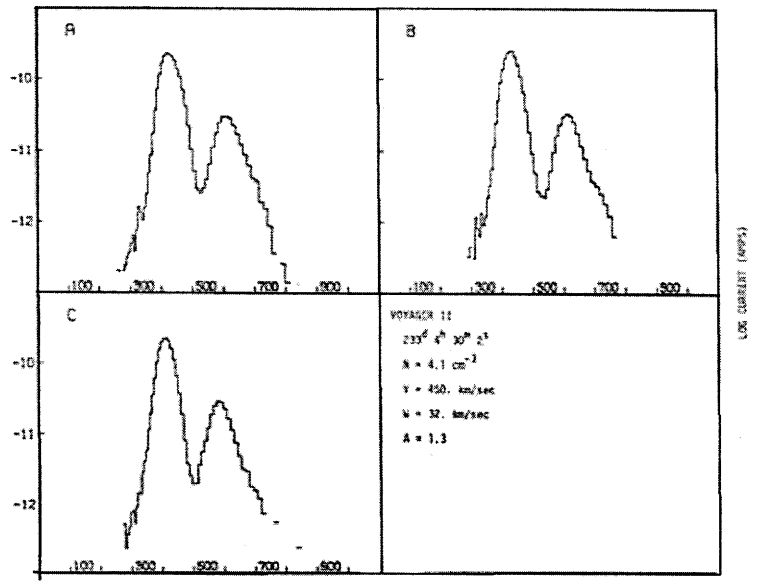

Figure 2-3: Sample energy-per-charge spectra from the three main Faraday cups [2].

$$F(v_n) \equiv \int_{-\infty}^{\infty} \int_{-\infty}^{\infty} dv_{t_1} dv_{t_2} f(v_n, v_{t_1}, v_{t_2}) \tag{2.11}$$

and conclude that the value of the reduced distribution function at the mean channel speed $\bar{v}_k$ is:

$$F(\bar{v}_k) = \frac{I_k}{qA\Delta v_k \bar{v}_k} \tag{2.12}$$

A sample measurement of the reduced distribution functions computed from equation 2.12 for the three main cup normals $\{\hat{n}_A, \hat{n}_B, \hat{n}_C\}$, is shown in Figure 2-3. The ion current displays two clear peaks: one for the proton population, and one for the alpha population (which is about 1/20 as abundant). The alpha population appears to be centered at twice the mean velocity of the protons (shown on a log scale), but in fact the protons and the alphas have equal bulk velocities. The shifted alpha peak in the spectrum is merely an artifact of the channels representing energy-per-charge, and with four times the mass and twice the charge, the alphas have twice the energy-per-charge as the protons (at equal velocity). The separation of the two peaks in this example allows us to easily pick out the proton population, but the proton and alpha populations are not always so distinguishable.

2.3 Bulk Velocity

Once we have the reduced distribution function along a cup normal, our next task is to compute the bulk velocity V_n represented by such a distribution. There are two common ways to do this, and each way is appropriate to a different situation.

2.3.1 Maxwellian Fits

One way to compute the bulk velocity is by assuming that the distribution is Maxwellian (i.e. thermal equilibrium has been achieved):

$$F(v_n) = n\sqrt{\frac{m}{2\pi kT}}\exp\left[-\frac{m}{2kT}(v_n - V_n)^2\right] \tag{2.13}$$

where n is the density and T is the temperature. We can then fit this form to the measured $F(\bar{v}_k)$ from Equation 2.12 by least-squares and determine the best fit parameters n, T, and V_n. The advantage of this method is that it allows us to scale the distribution function by an analytic correction factor $1/G(\vec{v})$ and thus obtain reliable results in situations where the assumption that $f(\vec{v})G(\vec{v}) \approx f(\vec{v})$ breaks down. The disadvantage is that it assumes the distribution function to be Maxwellian, which is not always the case, especially in the heliosheath.

2.3.2 Moments Calculation

The other way to compute the bulk velocity is from its definition as the first moment of the velocity distribution function. For *any* $f(\vec{v})$, we have

$$\begin{aligned} \vec{V} &\equiv \frac{1}{n}\int_{-\infty}^{\infty}\int_{-\infty}^{\infty}\int_{-\infty}^{\infty}\vec{v}\,f(\vec{v})d^3v \\ \longrightarrow V_n &= \frac{1}{n}\int_{-\infty}^{\infty}v_nF(v_n)dv_n \end{aligned} \tag{2.14}$$

where

$$\begin{aligned} n &\equiv \int_{-\infty}^{\infty}\int_{-\infty}^{\infty}\int_{-\infty}^{\infty}f(\vec{v})d^3v \\ \longrightarrow n &= \int_{-\infty}^{\infty}F(v_n)dv_n \end{aligned} \tag{2.15}$$

In terms of our discrete channels, this becomes

$$\begin{aligned} V_n &= \frac{1}{n}\sum_k v_k F(\bar{v}_k)\Delta v_k \\ &= \frac{1}{nqA}\sum_k I_k \end{aligned} \tag{2.16}$$

where

$$\begin{aligned} n &= \sum_k F(\bar{v}_k)\Delta v_k \\ &= \frac{1}{qA}\sum_k \frac{I_k}{\bar{v}_k} \end{aligned} \tag{2.17}$$

or just

$$V_n = \frac{\sum I_k}{\sum I_k/\bar{v}_k} \tag{2.18}$$

2.4 From Cup Normals to Spacecraft Axes

Once we have the bulk velocities V_A^{FC}, V_B^{FC}, and V_C^{FC} along the three Faraday cup normals, we want to transform them into an orthonormal basis — namely, that of the spacecraft axes. This can be done with a single matrix, as will be shown here.

In terms of the spacecraft orthonormal basis vectors $\{\hat{x}_{\text{SC}}, \hat{y}_{\text{SC}}, \hat{z}_{\text{SC}}\}$, the Faraday cup normals are given by:

$$\hat{A}_{\text{FC}} = -\hat{x}_{\text{SC}}\sin\theta_1\cos\theta_2 - \hat{y}_{\text{SC}}\sin\theta_1\cos\theta_3 - \hat{z}_{\text{SC}}\cos\theta_1 \tag{2.19}$$

$$\hat{B}_{\text{FC}} = \hat{x}_{\text{SC}}\sin\theta_1\cos\theta_2 - \hat{y}_{\text{SC}}\sin\theta_1\cos\theta_3 - \hat{z}_{\text{SC}}\cos\theta_1 \tag{2.20}$$

$$\hat{C}_{\text{FC}} = \hat{y}_{\text{SC}}\sin\theta_1 - \hat{z}_{\text{SC}}\cos\theta_1 \tag{2.21}$$

where $\theta_1 = 20°$, $\theta_2 = 30°$, and $\theta_3 = 60°$ [2]. We can invert these equations to obtain:

$$\hat{x}_{\text{SC}} = \frac{\hat{n}_B - \hat{n}_A}{2\sin\theta_1\cos\theta_2} \tag{2.22}$$

$$\hat{y}_{\text{SC}} = \frac{\hat{n}_C - \frac{1}{2}(\hat{n}_A + \hat{n}_B)}{\sin\theta_1(1+\cos\theta_3)} \tag{2.23}$$

$$\hat{z}_{\text{SC}} = -\frac{\frac{1}{2}(\hat{n}_A + \hat{n}_B) + \hat{n}_C\cos\theta_3}{\cos\theta_1(1+\cos\theta_3)} \tag{2.24}$$

Therefore the wind velocity in spacecraft coordinates, in terms of the measurements $(V_A^{\rm FC}, V_B^{\rm FC}, V_C^{\rm FC})$ taken along the Faraday cup normals, is given by:

$$V_x^{\rm SC} = \frac{V_B^{\rm FC} - V_A^{\rm FC}}{2\sin\theta_1\cos\theta_2} \tag{2.25}$$

$$V_y^{\rm SC} = \frac{V_C^{\rm FC} - \frac{1}{2}(V_A^{\rm FC} + V_B^{\rm FC})}{\sin\theta_1(1+\cos\theta_3)} \tag{2.26}$$

$$V_z^{\rm SC} = -\frac{\frac{1}{2}(V_A^{\rm FC} + V_B^{\rm FC}) + V_C^{\rm FC}\cos\theta_3}{\cos\theta_1(1+\cos\theta_3)} \tag{2.27}$$

Or, in matrix notation,

$$\vec{V}^{\rm SC} = M_{\rm FC}^{\rm SC}\vec{V}^{\rm FC} \tag{2.28}$$

where

$$M_{\rm FC}^{\rm SC} = \begin{pmatrix} \frac{-1}{2\sin\theta_1\cos\theta_2} & \frac{1}{2\sin\theta_1\cos\theta_2} & 0 \\ \frac{-1}{2\sin\theta_1(1+\cos\theta_3)} & \frac{-1}{2\sin\theta_1(1+\cos\theta_3)} & \frac{1}{\sin\theta_1(1+\cos\theta_3)} \\ \frac{-1}{2\cos\theta_1(1+\cos\theta_3)} & \frac{-1}{2\cos\theta_1(1+\cos\theta_3)} & \frac{-1}{\cos\theta_1(1+\cos\theta_3)} \end{pmatrix}$$

is the transformation matrix from cup to spacecraft coordinates. From the spacecraft axes, the velocity data is then rotated into one of the heliocentric coordinate systems described in section 3.

Chapter 3

Coordinate Systems

In this section we discuss two coordinate systems that have traditionally been used to describe observations in the solar system, and then introduce a new system which is appropriate for the heliosheath.

3.1 Ecliptic

Ecliptic coordinate systems are oriented with the z-axis normal to the earth's orbit (the ecliptic plane). Since the ecliptic plane is not constant from year to year, space scientists typically use the orbit of 1950 as the fundamental — this is called the ECL50 system. ECL50 comes in two versions: earth-centered and sun-centered. The Voyager program uses sun-centered ECL50, so we will define only this system here, and drop the modifier altogether.

The cartesian basis vectors in ECL50 are:

- $\hat{z}_{\text{ECL50}} \equiv \hat{\omega}_{\oplus}$, where $\vec{\omega}_{\oplus}$ is the angular velocity of Earth's orbit.
- $\hat{x}_{\text{ECL50}}$, which lies along the intersection of the ecliptic with the equatorial plane of the earth.
- $\hat{y}_{\text{ECL50}} = \hat{z}_{\text{ECL50}} \times \hat{x}_{\text{ECL50}}$, which completes the right-handed system.

3.2 Heliographic

Heliographic systems are oriented with the z-axis normal to the sun's rotational equator (the heliographic plane). Again, there are at least two versions of the heliographic system that are common in the space sciences: a cartesian version and a curvilinear version. We discuss each of them here.

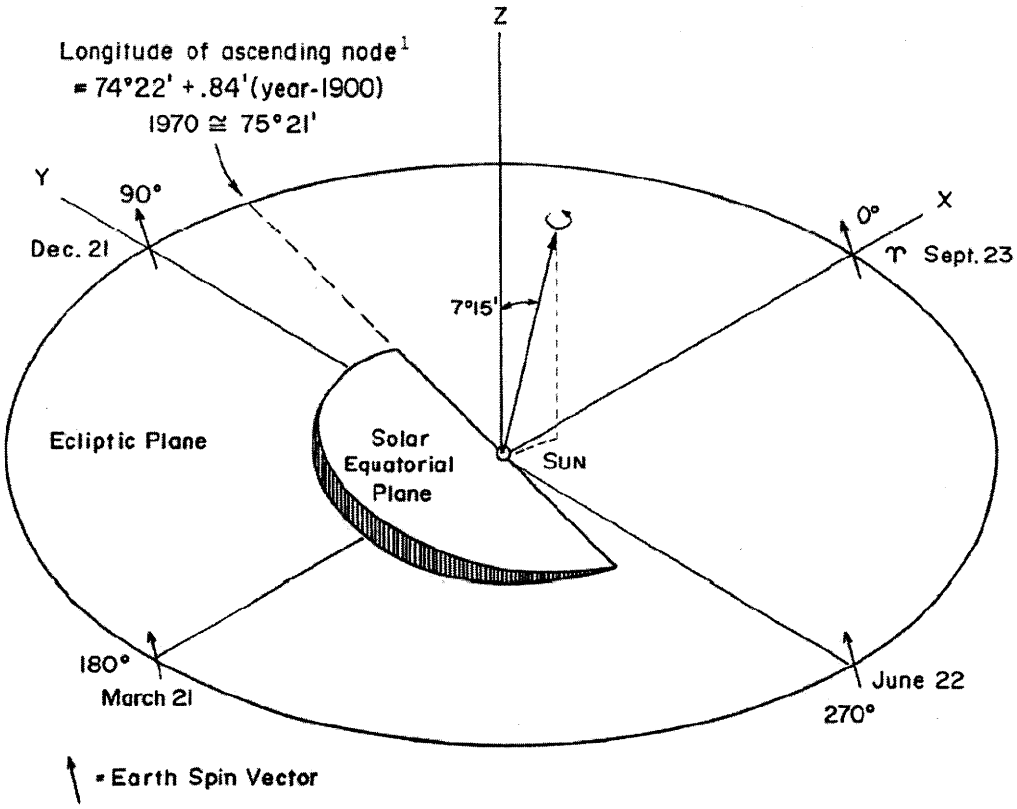

Figure 3-1: The ECL50 and Heliographic coordinate systems [7].

The cartesian basis vectors in the heliographic system are:

- $\hat{z}_{\mathrm{HG}} \equiv \hat{\omega}_{\odot}$, where $\vec{\omega}_{\odot}$ is the angular velocity of the sun's rotation.
- $\hat{x}_{\mathrm{HG}}$, which lies parallel to the intersection of heliographic and ecliptic planes and points toward the *ascending* node.
- $\hat{y}_{\mathrm{HG}} = \hat{z}_{\mathrm{HG}} \times \hat{x}_{\mathrm{HG}}$, which completes the right-handed system.

The relation between the ecliptic and heliographic systems is shown in Figure 3-1. A curvilinear basis is also common in the heliographic system. Its basis vectors are:

- $\hat{R}_{\mathrm{HG}}$, the *radial* direction, defined as the the sun-to-spacecraft unit vector.
- $\hat{T}_{\mathrm{HG}} = \hat{\omega}_{\odot} \times \hat{R}_{\mathrm{HG}} / |\hat{\omega}_{\odot} \times \hat{R}_{\mathrm{HG}}|$, the *tangential* direction.
- $\hat{N}_{\mathrm{HG}} = \hat{R}_{\mathrm{HG}} \times \hat{T}_{\mathrm{HG}}$, the *normal* direction, which completes the right-handed system.

The longitudinal meridian coincides with $\hat{x}_{\text{HG}}$ and the ascending node. The RTN system should not be confused with the traditional $\{\hat{r}, \hat{\theta}, \hat{\phi}\}$ spherical polar system, with which it bears many similarities but one crucial difference — the bases differ by a sign:

$$\hat{R} = \hat{r} \tag{3.1}$$

$$\hat{T} = \hat{\phi} \tag{3.2}$$

$$\hat{N} = -\hat{\theta} \tag{3.3}$$

notice that an odd permutation between the ordered triplets preserves the right-handedness of both bases.

3.3 Interstellar Heliospheric

We now introduce a coordinate system which we call Interstellar Heliospheric Coordinates (IHC). IHC is a heliocentric system which has its z-axis pointed toward the interstellar wind stagnation point. That is,

$$\hat{z}_{\text{IHC}} \equiv -\overrightarrow{V}_{\text{ISW}}/|\overrightarrow{V}_{\text{ISW}}| \tag{3.4}$$

where $\overrightarrow{V}_{\text{ISW}}$ is the interstellar wind velocity. Lallement et al. [4] found the direction to the stagnation point to be at ecliptic latitude $\beta = 9.0°$ and longitude $\lambda = 252.2°$. Using these values, the components of the IHC z-axis, in ecliptic coordinates, are:

$$(x_{\text{IHC}}, y_{\text{IHC}}, z_{\text{IHC}}) = (\cos\beta\cos\lambda, \cos\beta\sin\lambda, \sin\beta) \tag{3.5}$$

The x-axis is chosen to lie in the heliographic plane:

$$\hat{x}_{\text{IHC}} \equiv \hat{z}_{\text{IHC}} \times \hat{\omega}_{\odot}/|\hat{z}_{\text{IHC}} \times \hat{\omega}_{\odot}| \tag{3.6}$$

and the y-axis completes the right-handed system:

$$\hat{y}_{\text{IHC}} \equiv \hat{z}_{\text{IHC}} \times \hat{x}_{\text{IHC}} \tag{3.7}$$

From this, the spherical polar system is constructed in the usual way:

- $\hat{r}_{\text{IHC}}$ is the sun-to-spacecraft displacement vector
- $\hat{\phi}_{\text{IHC}} \equiv \hat{z}_{\text{IHC}} \times \hat{r}_{\text{IHC}}/|\hat{z}_{\text{IHC}} \times \hat{r}_{\text{IHC}}|$, and

- $\hat{\theta}_{\text{IHC}} \equiv \hat{\phi}_{\text{IHC}} \times \hat{r}_{\text{IHC}}$

The advantage of the IHC system is that it allows us to easily distinguish the effects of the interstellar medium from those which originate in the heliosphere: Interstellar effects should manifest themselves in the $r\theta$ planes and remain relatively free of ϕ dependence.

Chapter 4

Results

4.1 Data

Figure 4-1 shows the heliosheath velocities in RTN and IHC coordinates. In each system we see a sharp drop in radial velocity and a corresponding excitation in the transverse velocities around decimal year 2007.65. This is the crossing of the termination shock. After this, the spacecraft is in the heliosheath, which displays considerable variation; each velocity component takes on a base value and fluctuates about that value. Then, around decimal year 2008.6, we see a transient event which drastically affects nearly every component in the system. The remainder of this section is devoted to analyzing the steady state flows and variations observed in the heliosheath throughout the year 2008, with particular focus on the transient event of day 220.

4.2 Analysis

4.2.1 Steady State Flows

If we exclude the transient event (the period 2008.5–2008.7), and take the average value of each IHC velocity component over the rest of 2008, we get:

$$\langle V_r^{\text{IHC}} \rangle = (133.30 \pm 0.05) \text{ km/s} \tag{4.1}$$

$$\langle V_\theta^{\text{IHC}} \rangle = (54.33 \pm 0.07) \text{ km/s} \tag{4.2}$$

$$\langle V_\phi^{\text{IHC}} \rangle = (28.97 \pm 0.06) \text{ km/s} \tag{4.3}$$

where the errors are the standard error on the mean. The heliosheath plasma flow takes on a strongly positive θ_{IHC} component in accordance with the predicted influence

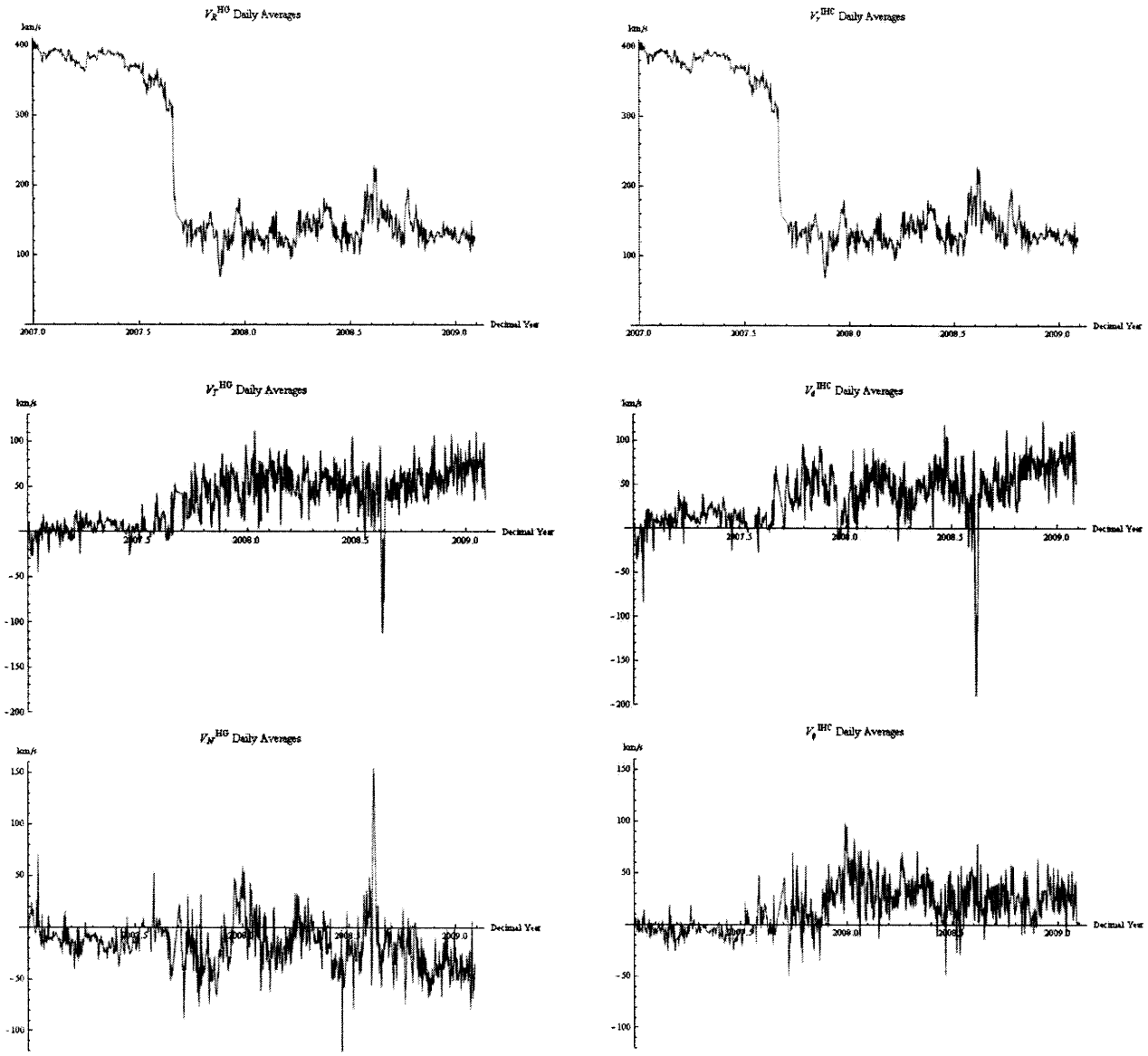

Figure 4-1: Plasma velocities measured by Voyager 2 as it crossed the termination shock. On the left we have the heliographic RTN components of velocity, and on the right, the IHC components.

of the interstellar medium discussed in Section 1.1. The ϕ_{IHC} component is also consistently positive, albeit less so than the θ_{IHC} component. This is a puzzling effect which requires further study.

We can also ask in which direction the flow is most (and least) constant by considering the variance matrix for the IHC velocity field:

$$\sigma_{ij}^2 \equiv \langle V_i V_j \rangle - \langle V_i \rangle \langle V_j \rangle \tag{4.4}$$

If we again exclude the transient event, this is:

$$\sigma_{ij}^2 = \begin{pmatrix} 293.6 & -126.8 & 30.98 \\ -126.8 & 631.1 & -121.6 \\ 30.98 & -121.6 & 387.3 \end{pmatrix} \text{(km/s)}^2$$

which has the following eigenvalues and eigenvectors:

$$\lambda_1 = 720.5 \text{ (km/s)}^2 \longrightarrow \vec{e}_1 = (0.29, -0.89, 0.35) \tag{4.5}$$

$$\lambda_2 = 341.1 \text{ (km/s)}^2 \longrightarrow \vec{e}_2 = (-0.20, 0.30, 0.93) \tag{4.6}$$

$$\lambda_3 = 250.4 \text{ (km/s)}^2 \longrightarrow \vec{e}_3 = (0.94, 0.34, 0.09) \tag{4.7}$$

The eigenvectors of the variance matrix tell us the direction (in IHC coordinates, in this case) in which we can expect to see the variance specified by the corresponding eigenvalues. We find that, in the heliosheath, the eigenvectors of the variance matrix are very nearly the basis vectors of the IHC system, which is a testament to its physical relevance. The least variance is in approximately the ϕ_{IHC} direction and the greatest variance is in approximately the θ_{IHC} direction, which is to be expected from variations in the interstellar wind.

4.2.2 Transient Event

The transient event that occurred on day 220 of 2008 represents a dramatic reversal of flow direction for several velocity components, in addition to nearly a doubling of the scalar wind speed. Nothing of its magnitude has since been observed in the heliosheath at the time of writing (May 2009). What could have caused such an event?

One possibility we investigated is that the transient event might have been caused by some violent solar activity, like a coronal mass ejection. To test this hypothesis, we tried to correlate the event with any signatures in the solar wind speed measured by the WIND satellite, which is stationed at the L1 Lagrangian point (helioradius ≈ 1

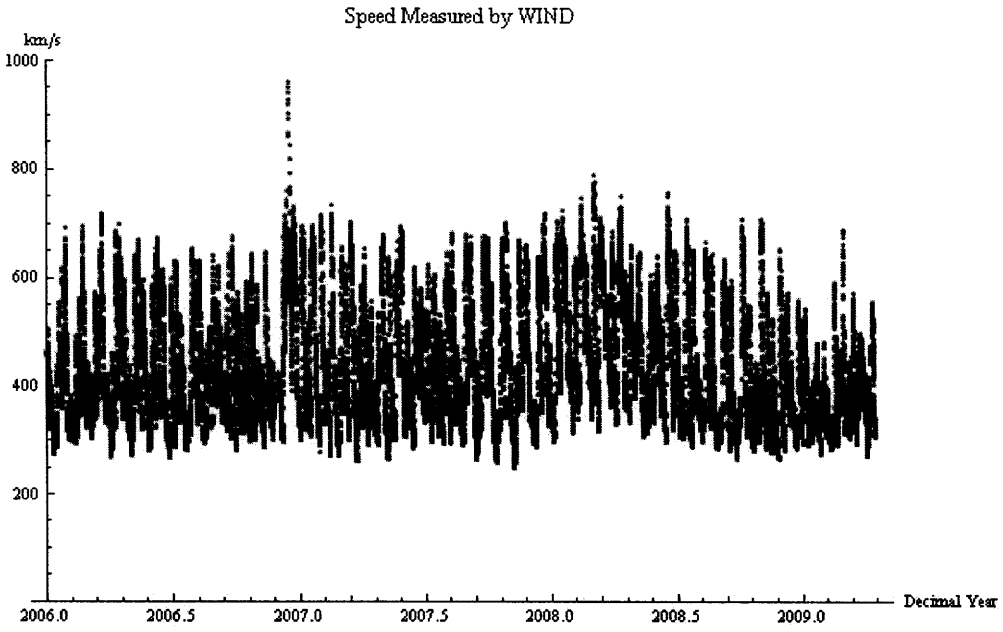

Figure 4-2: Solar wind speed measured at L1 by the WIND satellite.

AU). The solar wind speed measured by WIND over the past three years is shown in Figure 4-2.

We see a suspicious-looking event in which solar wind speed spiked up to 962 km/s at decimal year 2006.96. This is about 1.66 years earlier than the transient event in question was observed by Voyager 2 at a distance of 86.6 AU. At a speed of 962 km/s, this burst of solar wind would have reached the heliosheath in about 0.4 years, far too rapidly for this hypothesis to hold. Even if we assume that the burst was immediately slowed to the average solar wind speed of about 400 km/s after its encounter with WIND, it would still reach the heliosheath in about 1 year, much less than the observed time delay. It is therefore doubtful that the two events are correlated. Nevertheless, the WIND data during this period would merit further study if some other mode of influence could be identified.

So what can we say about 2008 transient? Referring back to Figure 4-1, we see that the event, which appeared in heliographic RTN coordinates as a sharp drop in the tangential component and a spike in the normal component, manifests itself in IHC as a purely θ-directed effect. Thus a heliographically random event is given significance in light of the interstellar influence: the transient can be described as a rush of shocked solar wind *toward* the interstellar wind stagnation point, possibly due to inhomogeneities in the Local Insterstellar Cloud.

Chapter 5

Conclusions

The Interstellar Heliospheric Coordinate (IHC) system has demonstrated a number of advantages over the heliographic system in the description of heliosheath-based observations. It simply and naturally expresses the effect of shear momentum transfer from the interstellar wind into a consistently positive velocity V_θ^{IHC} of plasma directed down the heliotail. Its basis has been shown to coincide with the eigenvectors of the variance matrix measured by Voyager 2, a fact which strongly hints at its physical significance in the heliosheath. And perhaps most remarkably, it has shed light on the nature of a strong transient event which could be related to inhomogeneities in the Local Insterstellar Cloud.

Appendix A

Conventions and Definitions

A.1 Vector Notation

Throughout this thesis we frequently relate vector components in different coordinate systems using matrix transformations. In order to keep clear the many labels adorning the vectors, we have adopted a consistent notational convention, which is explained here.

An arbitrary vector is represented by an arrow-topped variable and a superscript denoting the coordinate system that its components reflect. The components are labeled with the same variable (arrow-free), the same superscript, and an additional subscript indicating which component it represents. For example, the wind velocity vector in spacecraft coordinates is written $\overrightarrow{V}^{\mathrm{SC}}$, and its components are $(V_x^{\mathrm{SC}}, V_y^{\mathrm{SC}}, V_z^{\mathrm{SC}})$. Basis vectors are represented by a carat-topped variable subscripted by the coordinate system to which they belong. For example, the spacecraft coordinate system has basis vectors $\{\hat{x}_{\mathrm{SC}}, \hat{y}_{\mathrm{SC}}, \hat{z}_{\mathrm{SC}}\}$. The notation is summarized by the following expression for the wind velocity in spacecraft coordinates:

$$\overrightarrow{V}^{\mathrm{SC}} = V_x^{\mathrm{SC}}\hat{x}_{\mathrm{SC}} + V_y^{\mathrm{SC}}\hat{y}_{\mathrm{SC}} + V_z^{\mathrm{SC}}\hat{z}_{\mathrm{SC}} \tag{A.1}$$

Occasionally we need to distinguish vectors of the same variable and coordinate system; in these cases, we add a subscript to the vectors themselves, as in $\overrightarrow{V}_{\mathrm{ab}}^{\mathrm{ECL50}}$ for the aberrated wind velocity in ECL50 coordinates.

A.2 Coordinate Systems: Quick Reference

The following table collects the variables and labeling conventions used throughout this thesis to refer to the various coordinate systems.

Coordinate System	Abbreviation	Basis Vectors	Components of $\vec{V}$
Faraday Cups	FC	$\hat{A}_{\rm FC}$, $\hat{B}_{\rm FC}$, $\hat{C}_{\rm FC}$	$V_A^{\rm FC}$, $V_B^{\rm FC}$, $V_C^{\rm FC}$
Spacecraft Axes	SC	$\hat{x}_{\rm SC}$, $\hat{y}_{\rm SC}$, $\hat{z}_{\rm SC}$	$V_x^{\rm SC}$, $V_y^{\rm SC}$, $V_z^{\rm SC}$
Ecliptic 1950	ECL50	$\hat{x}_{\rm ECL50}$, $\hat{y}_{\rm ECL50}$, $\hat{z}_{\rm ECL50}$	$V_x^{\rm ECL50}$, $V_y^{\rm ECL50}$, $V_z^{\rm ECL50}$
Heliographic	HG	$\hat{x}_{\rm HG}$, $\hat{y}_{\rm HG}$, $\hat{z}_{\rm HG}$ $\hat{R}_{\rm HG}$, $\hat{T}_{\rm HG}$, $\hat{N}_{\rm HG}$	$V_x^{\rm HG}$, $V_y^{\rm HG}$, $V_z^{\rm HG}$ $V_R^{\rm HG}$, $V_T^{\rm HG}$, $V_N^{\rm HG}$
Interstellar Heliospheric	IHC	$\hat{r}_{\rm IHC}$, $\hat{\theta}_{\rm IHC}$, $\hat{\phi}_{\rm IHC}$	$V_r^{\rm IHC}$, $V_\theta^{\rm IHC}$, $V_\phi^{\rm IHC}$

Bibliography

[1] W. I. Axford, , and S. T. Suess. Spacecraft to explore the outer heliosphere. *Eos Trans. AGU*, 75(50):587, 1994.

[2] John W. Belcher. Voyager plasma science instrument. Unpublished, March 2009.

[3] H.S. Bridge, J.W. Belcher, R.J. Butler, A.J. Lazarus, A.M. Mavretic, J.D.Sullivan, G.L. Siscoe, and V.M. Vasyliunas. The plasma experiment on the 1977 voyager mission. *Space Science Reviews*, 21:259–287, 1977. DOI: 10.1007/BF00211542.

[4] R. Lallement, E. Quemerais, J.L. Bertaux, S. Ferron, D. Koutroumpa, and R. Pellinen. Deflection of interstellar neutral hydrogen flow across the heliospheric surface. *Science*, 307:1447–1449, 2005. DOI: 10.1126/science.1107953.

[5] C. Marton, H.R. Griem, and R.H. Lovberg. *Plasma Physics*, volume 9 of *Methods of Experimental Physics.* Academic Press, New York, 1971. Part B.

[6] J.D. Richardson, J.C. Kasper, C. Wang, J.W. Belcher, and A.J. Lazarus. Cool heliosheath plasma and deceleration of the upstream solar wind at the termination shock. *Nature Letters*, 454:63–66, 2008. DOI: 10.1038/nature07024.

[7] J.D. Richardson, E.C. Stone, J.C. Kasper, J.W. Belcher, and R.B. Decker. Plasma flows in the heliosheath. *Geophysical Research Letters*, 36, 2009. DOI: 10.1029/2009GL038421.